Linear Dynamic Viscoelastic Properties of Functionalized Block Copolymer/Organoclay Nanocomposites

Kyung Min Lee and Chang Dae Han*

Department of Polymer Engineering, The University of Akron, Akron, Ohio 44325-0301

Received May 28, 2002

ABSTRACT: Linear dynamic viscoelastic properties of functionalized block copolymer/organoclay nanocomposites were investigated. The organoclay employed (Cloisite 30B, Southern Clay Products) is natural clay modified with methyl, tallow, bis(2-hydroxyethyl), quaternary ammonium chloride (MT2EtOH). Nanocomposites were prepared by solution blending Cloisite 30B with a polystyrene-*block*-hydroxylated polyisoprene (SIOH diblock) copolymer having hexagonally packed cylindrical microdomains of polystyrene (PS). For comparison, nanocomposites were also prepared by solution blending Cloisite 30B with a polystyrene-*block*-polyisoprene (SI diblock) copolymer having lamellar microdomain structure. It was found from the linear dynamic viscoelastic measurements that the dynamic storage modulus (G') and complex viscosity ($|\eta^*|$) of 95/5 SIOH/Cloisite 30B nanocomposite *increased* as the temperature was increased from 170 to 240 °C, while the G' and $|\eta^*|$ of 95/5 SI/Cloisite 30B nanocomposite *decreased* as the temperature was increased from 90 to 125 °C, where 95/5 refers to the weight percent of the constituent components. In situ Fourier transform infrared spectroscopy indicated that hydrogen bonding persisted in the 95/5 SIOH/Cloisite 30B nanocomposite at temperatures as high as 240 °C, the highest experimental temperature employed, while no measurable hydrogen bonding existed in the 95/5 SI/Cloisite 30B nanocomposite at temperatures ranging from 30 to 240 °C. Thus, it is concluded that the rather unusual temperature dependence of G' and $|\eta^*|$ for the 95/5 SIOH/Cloisite 30B nanocomposite is attributable to an enhanced dispersion, and thus larger surface areas available, of the silicate layers of clay aggregates as the temperature is increased. It is speculated that the enhanced dispersion of the silicate layers of organoclay aggregates occurs due to the compatibilization, via hydrogen bonding, between the hydroxyl groups in SIOH and the polar groups in MT2EtOH on the surfaces of organoclay aggregates. It was found from both the dynamic frequency sweep and isochronal dynamic temperature sweep experiments that the order−disorder transition temperature (T_{ODT}) of the 95/5 SIOH/Cloisite 30B nanocomposite exceeded 240 °C, the highest experimental temperature employed, while the T_{ODT} of the neat SIOH diblock copolymer was 198 °C and the T_{ODT} of the 95/5 SI/Cloisite 30B nanocomposites was 115 °C, the *same* as that of the neat SI diblock copolymer. The above observation, once again, suggests that strong attractive interactions exist, via hydrogen bonding, between the hydroxyl groups in SIOH and the polar functional groups in MT2EtOH of the chemically modified clay. Studies using X-ray diffraction and transmission electron microscopy support the conclusions drawn above.

1. Introduction

In recent years, nanocomposites composed of a thermoplastic polymer and the exfoliated silicate layers of organoclay have attracted much attention from both industry and academia, because they offer very unique mechanical and physical properties (e.g., high strength, high modulus, high heat distortion temperature) that are not readily available from conventional particulate-filled polymers. As in the preparation of polymer blends having improved mechanical properties, compatibility is essential in the preparation of nanocomposites; i.e., since the silicate layers of the organoclay have polar groups, they are compatible only with polymers containing polar functional groups. This is the reason that nylon-6/organoclay nanocomposites have markedly improved mechanical properties,[1−6] because nylon-6 has amine end groups that can easily form hydrogen bonds with the hydroxyl or carboxyl groups grafted onto the surface of the silicate layers of the organoclay. Other thermoplastic polymers, such as polypropylene (PP),[7−11] polystyrene (PS),[12,13] and poly(ethylene oxide) (PEO),[14,15] also have been employed as the matrix in nanocomposites. When a thermoplastic polymer does not have functional group(s), chemical modification of the polymer or use of a compatibilizing agent is necessary for preparing useful nanocomposites with the silicate layers of organoclay. The preparation of PP/organoclay nanocomposites with the aid of maleic anhydride functionalized polypropylene oligomers as a compatibilizer is a good example of such an effort, because PP has no polar functional group. For the fundamental concepts for the development of thermoplastic polymer/organoclay nanocomposites, the readers are referred to the recent review articles.[16−19]

The processing of nanocomposites requires information on their rheological properties. Very recently, several research groups reported on the rheological behavior of thermoplastic polymer/organoclay nanocomposites; namely, some investigators[20−22] reported on oscillatory shear flow properties while others[23] reported on transient and/or steady shear flow properties. On the other hand, only a few studies have reported on the rheological behavior of block copolymer/organoclay nanocomposites. Ren et al.[24] reported on linear dynamic viscoelastic properties of nanocomposites consisting of a disordered polystyrene-*block*-polyisoprene (SI diblock) copolymer and organoclay. Subsequently, they[25] reported on steady-state shear properties of the same nanocomposites. In view of the fact that the SI diblock copolymers employed by them did not have any functional group, no significant compatibility (or interaction) is expected between the block copolymer and organoclay. Significantly improved mechanical properties of block

10.1021/ma020816f CCC: $25.00
Published on Web 01/07/2003

copolymer/organoclay nanocomposites may be obtained through significant dispersion (exfoliation) of organoclay aggregates by a functionalized block copolymer.

Very recently, we prepared nanocomposites by mixing chemically modified clay (hereafter referred to as organoclay) with a polystyrene-*block*-hydroxylated polyisoprene (SIOH diblock) copolymer having hexagonally packed, cylindrical microdomains of PS and then investigated their linear dynamic viscoelastic properties. For comparison, we also investigated linear dynamic viscoelastic properties of nanocomposites consisting of the same organoclay and a polystyrene-*block*-polyisoprene (SI diblock) copolymer having lamellar microdomain structure. The organization of this paper is as follows. We first present linear dynamic viscoelastic properties of block copolymer/organoclay nanocomposites. Then, from the measurements of linear dynamic viscoelastic properties, we present evidence suggesting that the SIOH is very effective at achieving a significant degree of dispersion of the organoclay aggregates, while the SI diblock copolymer is not. Finally, we present the results of X-ray diffraction and transmission electron microscopy, supporting the results obtained from the linear dynamic viscoelastic measurements.

2. Experimental Section

Materials and Sample Preparation. To prepare nanocomposites with a functionalized block copolymer, we employed an organoclay (Cloisite 30B, Southern Clay Products), which is a natural clay chemically modified with methyl, tallow, bis-(2-hydroxyethyl), quaternary ammonium chloride (MT2EtOH) with the chemical structure[26]

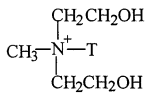

MT2EtOH

where N^+ denotes quaternary ammonium chloride and T denotes tallow consisting of 65% C18, 30% C16, and 5% C14. The rationale behind the choice of Cloisite 30B, among several other chemically modified clays available from Southern Clay Products, was that MT2EtOH in Cloisite 30B contains hydroxyl groups that match with the hydroxyl groups in the functionalized block copolymer we have synthesized, as described below.

In this study we prepared a functionalized block copolymer by introducing hydroxyl groups, via hydroboration/oxidation reactions,[27,28] into a low-molecular-weight SI diblock copolymer (SI-14/3), yielding a *hydroxylated* SI diblock copolymer (SI-14/3-OH). For this, we first synthesized SI-14/3, via anionic polymerization, in tetrahydrofuran (THF) as solvent and *sec*-butyllithium (*sec*-BuLi) as initiator using standard procedures. This resulted in PI blocks having the following microstructures: 34% 1,2-addition, 59% 3,4-addition, and 7% 1,4-addition. It should be mentioned that the reactivity of 1,2- and 3,4-additions in PI block to hydroboration/oxidation reactions is much greater than that of 1,4-addition in PI.[28] If an SI diblock copolymer is synthesized in cyclohexane as solvent, it will result in PI blocks having predominantly (94%) 1,4-addition and only 6% 3,4-addition. It is very difficult to obtain a high degree of hydroxylation from such an SI diblock copolymer. Using ^{1}H nuclear magnetic resonance (NMR) spectroscopy, we confirmed that all of the 1,2- and 3,4-additions of PI blocks in SI-14/3 were hydroxylated. The details of the preparation of the SI-14/3-OH diblock copolymer employed are described in our recent paper.[29] It should be mentioned that SI-14/3 is a homogeneous (disordered) diblock copolymer, while SI-14/3-OH is a microphase-separated diblock copolymer having hexagonally packed, cylindrical microdomains of PS.[29] SI-14/3-OH was used to prepare nanocomposites with a chemically modified clay. For comparison, we also synthesized a lamella-forming SI diblock copolymer (SI-10/9) to prepare nanocomposites with a chemically modified clay. Table 1 gives a summary of the molecular characteristics of the two SI diblock copolymers synthesized.

Table 1. Molecular Characteristics of the SI Diblock Copolymers Synthesized in This Study

sample code	M_n (g/mol)[a]	M_w/M_n[b]	PS (wt frac)[c]	morphology[d]
SI-10/9	1.94×10^4	1.02	0.54	lamellae
SI-14/3	1.70×10^4	1.08	0.84	homogeneous

[a] Determined from membrane osmometry. [b] Determined from GPC. [c] Determined from ^{1}H NMR spectroscopy. [d] Determined from TEM.

We prepared (SI-14/3-OH)/Cloisite 30B and (SI-10/9)/Cloisite 30B nanocomposites by solution blending, while vigorously stirring, in a cosolvent of THF/water at room temperature for 30 min, followed by slow evaporation under agitation. In the preparation of (SI-14/3-OH)/Cloisite 30B nanocomposites the amount of Cloisite 30B used was 1, 3, or 5 wt %. It should be mentioned that the amount of surfactant on the surface of the natural clay is 32 wt %, and thus the net amounts of clay are 0.68 wt % in the 99/1 (SI-14/3-OH)/Cloisite 30B nanocomposite, 2.04 wt % clay in the 97/3 (SI-14/3-OH)/Cloisite 30B nanocomposite, and 3.4 wt % clay in the 95/5 (SI-14/3-OH)/Cloisite 30B nanocomposite, where 95/5, for instance, refers to the weight percent of SI-14/3-OH and Cloisite 30B, respectively. Specifically, a predetermined amount of SI-14/3-OH was dissolved in a cosolvent of THF/H_2O (90:10 v:v), and then Cloisite 30B in a cosolvent of THF/H_2O was added slowly, while stirring, into the block copolymer solution. This mixture was evaporated slowly under constant stirring for 2 days. After the mixture of SI-14/3-OH and Closite 30B was dried completely in a vacuum oven at 50 °C for 1 day, it was in powder form. For rheological measurements, a thin film of about 0.1 mm thick was prepared by compression molding at 140 °C.

For comparison, we also prepared, via twin-screw extrusion (ZSK 53, Werner & Pfleiderer), calcium carbonate ($CaCO_3$)-filled polypropylene (PP) composites having 10, 20, or 40 wt % $CaCO_3$. The PP employed was a commercial grade (E115, Exxon Chemical), and the $CaCO_3$ (Thomson & Weinman) employed had an average particle size of 2.5 μm.

Rheological Measurements. An Advanced Rheometric Expansion System (ARES, Rheometric Scientific) with a parallel-plate fixture (8 mm diameter) was used to conduct dynamic frequency sweep experiments of the composites, measuring the storage and loss moduli (G' and G'') as functions of angular frequency (ω) (ranging from 0.01 to 100 rad/s) and temperature. A fixed strain of 0.04 was used to ensure that measurements were taken well within the linear viscoelastic range of the materials investigated. The frequency sweep experiment at a preset temperature lasted for about 45 min, while the temperature control was accurate to within ±1 °C. Dynamic temperature sweep experiments under isochronal conditions were also conducted at $\omega = 0.01$ rad/s during heating, where temperature was increased stepwise in 2 °C/min increments. All tests were conducted under a nitrogen atmosphere to avoid oxidative degradation of the samples.

Fourier Transform Infrared Spectroscopy (FTIR). Using a Fourier transform infrared spectrometer (16 PC FTIR, Perkin-Elmer), in-situ FTIR spectra were obtained at various temperatures ranging from 30 to 240 °C for neat block copolymer SI-14/3-OH, 95/5 (SI-14/3-OH)/Cloisite 30B nanocomposite, and 95/5 (SI-10/9)/Cloisite 30B nanocomposite. Spectral resolution was maintained at 4 cm^{-1}. The temperature was measured at the sample surface and controlled within ±1.0 °C using a proportional-integral-derivative controller. Specimens were maintained at a preset temperature for 5 min prior to data acquisition. Dry argon gas was used to purge the sample compartment in order to reduce the interference of water and carbon dioxide in the spectrum. Thin films suitable for FTIR were prepared by casting 2% (w/v) solution in THF directly on the KBr salt plate. Film thickness was adjusted, such that the maximum absorbance of any band was less than

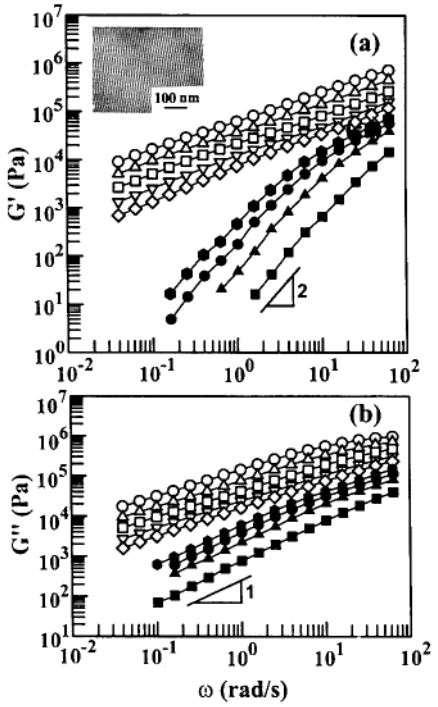

Figure 1. (a) Plots of log G' vs log ω and (b) log G'' vs log ω for SI-10/9 diblock copolymer at various temperatures: (○) 95, (△) 100, (□) 105, (▽) 109, (◇) 112, (●) 115, (▲) 118, (■) 121, and (▼) 125 °C. The inset gives a TEM image of SI-10/9 taken at room temperature.

1.0, at which the Beer−Lambert law is valid. It was slowly dried for 24 h in a fume hood until most of the solvent evaporated and then dried at 70 °C for a few days in a vacuum oven. Samples were then stored in a vacuum oven until use.

X-ray Diffraction. Using a Rigaku X-ray generator operated at 40 kV and 40 mA, X-ray diffraction patterns were obtained to determine the mean interlayer spacing of the (001) plane (d_{001}) for the organoclay (Cloisite 30B) and its nanocomposites with a block copolymer (SI-10/9 or SI-14/3-OH) prepared in this study. The X-ray beam was monochromatized to Cu Kα with a graphite crystal. The range of 2θ scanning of X-ray intensity employed was 1.5°−10°.

Transmission Electron Microscopy (TEM). TEM images of specimens were taken at room temperature. The ultrathin sectioning (50−70 nm) was performed cryoultramicrotomy at −80 °C for SI-10/9 and (SI-10/9)/Cloisite 30B nanocomposites and at room temperatures for SI-14/3-OH and (SI-14/3-OH)/Cloisite 30B nanocomposites using a Reichert Ultracut E low-temperature sectioning system. A transmission electron microscope (JEM1200EX 11, JEOL) operated at 120 kV was used to obtain images of the nanocomposite specimens.

3. Results and Discussion

Linear Dynamic Viscoelastic Properties of (SI-10/9)/Cloisite 30B Nanocomposites and $CaCO_3$-Filled Polypropylene Composites. To facilitate our discussion below, we first present linear dynamic viscoelastic properties of neat diblock copolymer SI-10/9. Figure 1a gives log G' vs log ω plots and Figure 1b gives log G'' vs log ω plots for SI-10/9 at various temperatures. As can be seen from the TEM image given in the inset of Figure 1a, SI-10/9 has lamellar microdomains. In Figure 1a we observe that values of G' are very large at low temperatures with a slope much less than 2 in the terminal region, indicating that the block copolymer exhibits linear dynamic viscoelasticity somewhere between solidlike and liquidlike states. Interestingly, as the temperature is increased to a certain critical temperature (115 °C), values of G' in the terminal region drop rapidly, and then the log G' vs log ω plot is shifted downward with a slope of 2 in the terminal region, characteristic of liquidlike behavior. On the other hand, Figure 1b shows that a change in the slope of log G'' vs log ω plot at 115 °C is very small.

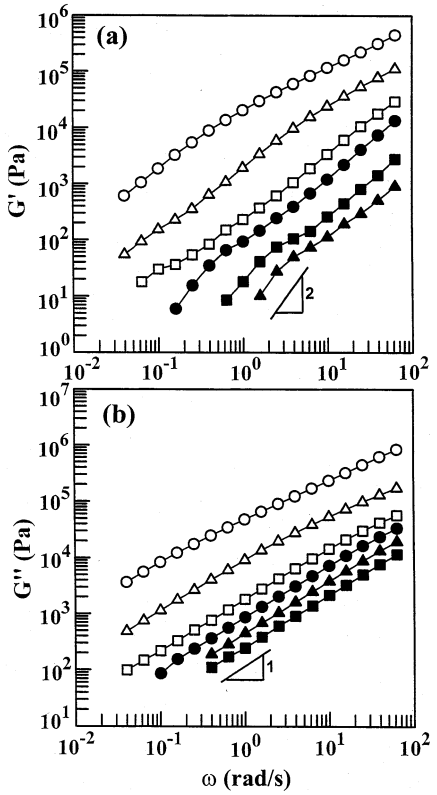

Figure 2. (a) Plots of log G' vs log ω and (b) log G'' vs log ω for 95/5 (SI-10/9)/Cloisite 30B nanocomposite at various temperatures: (○) 90, (△) 100, (□) 110, (●) 115, (▲) 120, and (■) 125 °C.

Figure 2a gives log G' vs log ω plots and Figure 2b gives log G'' vs log ω plots for 95/5 (SI-10/9)/Cloisite 30B nanocomposite at various temperatures. Comparison of Figure 2a with Figure 1a indicates that the addition of 5 wt % Cloisite 30B to SI-10/9 has changed drastically the temperature dependence of the log G' vs log ω plot. Specifically, *below* 115 °C the slope of the log G' vs log ω plot for the 95/5 (SI-10/9)/Cloisite 30B nanocomposite in the terminal region is much greater than that for the neat block copolymer SI-10/9, indicating that the nanocomposite behaves less solidlike as compared to the neat block copolymer SI-10/9. Also, comparison of Figure 2b with Figure 1b indicates that the log G'' vs log ω plot is not as sensitive to the addition of 5 wt % Cloisite 30B to SI-10/9 as the log G' vs log ω plot is. Of particular interest in Figure 2 is that in the terminal region at 115 °C and higher temperatures the log G' vs log ω plots have a slope of 2 and the log G'' vs log ω plots have a slope of 1, exhibiting liquidlike behavior, although the nanocomposite has 5 wt % Cloisite 30B. That is, at 115 °C and higher temperatures the linear dynamic viscoelastic behavior of the 95/5 (SI-10/9)/Cloisite 30B nanocomposite in the terminal region is *little* different from that of the neat block copolymer SI-10/9. Below we will explain the reason for this observation after presenting more experimental results.

Figure 3a gives log G' vs log G'' for the neat diblock copolymer SI-10/9 at various temperatures. It is seen

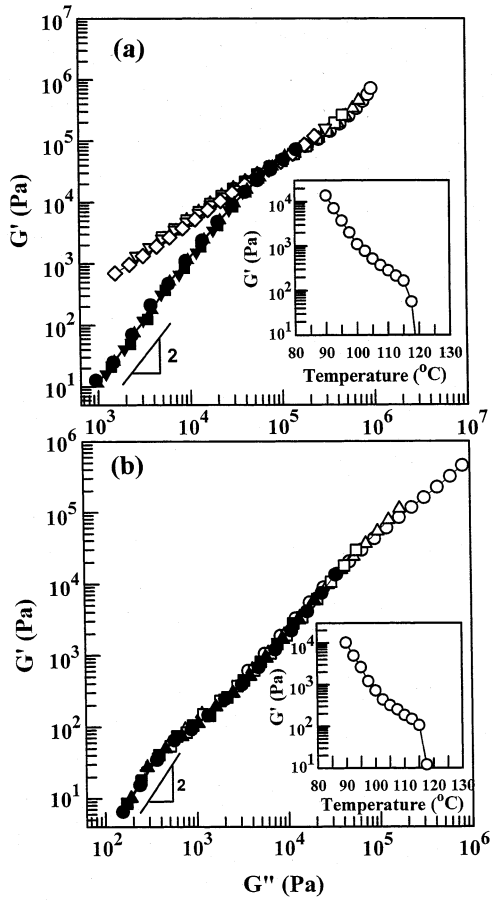

Figure 3. (a) Plots of log G' vs log G'' for SI-10/9 diblock copolymer at various temperatures: (○) 95, (△) 100, (□) 105, (▽) 109, (◇) 112, (●) 115, (▲) 118, (■) 121, and (▼) 125 °C. (b) Plots of log G' vs log G'' for 95/5 (SI-10/9)/Cloisite 30B nanocomposite at various temperatures: (○) 90, (△) 100, (□) 110, (●) 115, (▲) 120, and (■) 125 °C. The inset describes variations of G' with temperature during isochronal dynamic temperature sweep experiments at $\omega = 0.01$ rad/s.

in Figure 3a that the log G' vs log G'' plot at temperatures below ca. 115 °C has a slope much less than 2 and then shifts suddenly downward with a slope of 2 in the terminal region as the temperature is increased to 115 °C and higher. Following the rheological criterion[30] that the T_{ODT} of a block copolymer may be determined by the threshold temperature, during heating, at which the log G' vs log G'' plot begins to be independent of temperature and has a slope of 2 in the terminal region, we determine the T_{ODT} of SI-10/9 to be ca. 115 °C. The inset of Figure 3a describes the results of isochronal dynamic temperature sweep experiments at $\omega = 0.01$ rad/s. According to the rheological criterion[31] that the temperature at which G' begins to drop precipitously in the isochronal dynamic temperature sweep experiment signifies the onset of ODT, from the inset of Figure 3a we determine the T_{ODT} of SI-10/9 to be ca. 117 °C, which is very close to the T_{ODT} determined from the log G' vs log G'' plot. Note that two different rheological criteria give rise to virtually the identical value of T_{ODT} for the lamella-forming block copolymer SI-10/9. Earlier, a similar observation has been reported also for other lamella-forming block copolymers.[32−35]

Figure 3b gives log G' vs log G'' plots for 95/5 (SI-10/9)/Cloisite 30B nanocomposite. It is interesting to observe in Figure 3b that log G' vs log G'' plot for the 95/5 (SI-10/9)/Cloisite 30B nanocomposite is virtually independent of temperature over the entire range of temperatures tested, but the slope of the log G' vs log G'' plot is less than 2 for values of G'' above ca. 500 Pa and then becomes very close to 2 for $G'' \leq$ ca. 500 Pa at 115 °C and higher temperatures. According to the rheological criterion of Han and workers,[30] the temperature independence of log G' vs log G'' is *not* sufficient for one to claim that a block copolymer is in the disordered state; i.e., in addition to temperature independence, the log G' vs log G'' plot must have a slope of 2 in the terminal region for one to claim that a block copolymer is in the disordered state. Following such a rheological criterion, from Figure 3b we determine the T_{ODT} of the 95/5 (SI-10/9)/Cloisite 30B nanocomposite to be ca. 115 °C. Interestingly, the T_{ODT} determined from the log G' vs log G'' plot agrees very well with the temperature at which G' begins to drop precipitously in the isochronal dynamic temperature sweep experiment at $\omega = 0.01$ rad/s, the results of which are given in the inset of Figure 3b. The above observations lead us to conclude that the addition of 5 wt % organoclay to the neat block copolymer SI-10/9 did *not* change its T_{ODT}, suggesting that little interaction, physical or chemical, took place between the organoclay Cloisite 30B and the lamella-forming block copolymer SI-10/9. After all, this conclusion should not surprise us, because the block copolymer SI-10/9 does not have any functional group that can interact, physically or chemically, with the polar groups in the coupling agent, MT2EtOH, of Cloisite 30B.

Referring to Figure 3b, it may seem strange, at first glance, to observe that as expected from Figure 2, at 115 °C and higher temperatures (i.e., in the disordered state of SI-10/9) the slope of the log G' vs log G'' plots for the 95/5 (SI-10/9)/Cloisite 30B nanocomposite is very close to 2 in the terminal region (i.e., liquidlike behavior), although it contains 5 wt % Cloisite 30B. This is attributed to two factors: (i) the concentration of Cloisite 30B in the nanocomposite was *not* sufficiently high, and (ii) there were little or no physical or chemical interactions between Cloisite 30B and SI-10/9 in the 95/5 (SI-10/9)/Cloisite 30B nanocomposite. It should be remembered that 5 wt % Cloisite 30B consists of 3.4 wt % clay and 1.6 wt % organic coupling agent. As will be shown below, however, 5 wt % Cloisite 30B was found to be sufficiently high to give rise to the slope of log G' vs log G'' plots in the terminal region *less* than 2 when it is blended with the *functionalized* block copolymer SI-14/3-OH.

To help facilitate our discussion here, in this study we also investigated the linear dynamic viscoelastic properties of $CaCO_3$-filled polypropylene (PP) composites with varying concentrations of $CaCO_3$. Figure 4 gives (a) log G' vs log ω plots and (b) log G'' vs log ω plots for PP (the open symbols) and 40 wt % $CaCO_3$-filled PP composites (the filled symbols). It is seen that the slope of log G' vs log ω plots is very close to 2 for PP but much *less than* 2 for the 40 wt % $CaCO_3$-filled PP composites, and the slope of log G'' vs log ω plots is very close to 1 for PP but much *less than* 1 for the 40 wt % $CaCO_3$-filled PP composite. This observation now explains why in Figure 2 the 95/5 (SI-10/9)/Cloisite 30B nanocomposite in the disordered state of SI-10/9 (i.e., above the T_{ODT} of SI-10/9) has a slope of 2 in the terminal region of log G' vs log ω plots and a slope of 1 in the terminal region of log G'' vs log ω plots, i.e., 5 wt % of organoclay Cloisite 30B (3.4 wt % *net* clay), even if

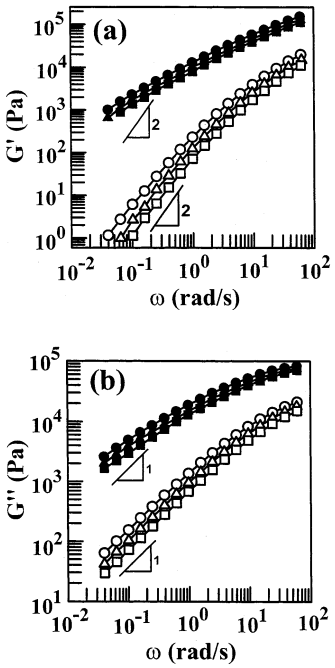

Figure 4. (a) Plots of log G' vs log ω and (b) plots of log G'' vs log ω for PP (open symbols) and 60/40 PP/$CaCO_3$ composite (filled symbols) at (○, ●) 190, (△, ▲) 210, and (□, ■) 230 °C.

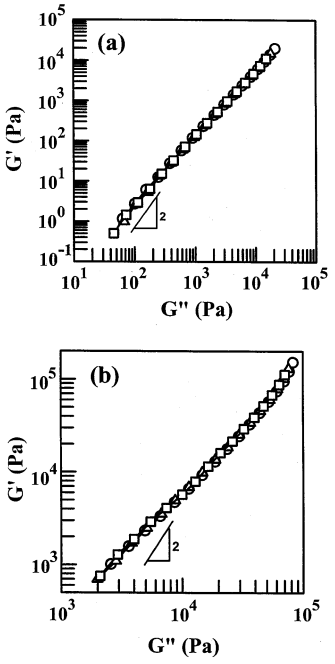

Figure 5. Plots of log G' vs log G'' at (○) 190, (△) 210, and (□) 230 °C for (a) PP and (b) 60/40 PP/$CaCO_3$ composite.

all of the platelets are fully exfoliated, was *not* sufficiently high to make the linear dynamic viscoelastic behavior of the 95/5 (SI-10/9)/Cloisite 30B nanocomposite deviate from liquidlike behavior. This is further demonstrated in Figure 5, in which we observe that the slope of log G' vs log G'' plots in the terminal region for the 40 wt % $CaCO_3$-filled PP composite is less than 2, while the slope of the log G' vs log G'' plots in the terminal region for PP is very close to 2.

Plots of log $|\eta^*|$ vs log ω for neat PP, 90/10, 80/20, and 60/40 PP/$CaCO_3$ composites at 190 °C are given in Figure 6, in which $|\eta^*|$ was calculated using the definition $|\eta^*| = [(G'/\omega)^2 + (G''/\omega)^2]^{1/2}$. It should be mentioned

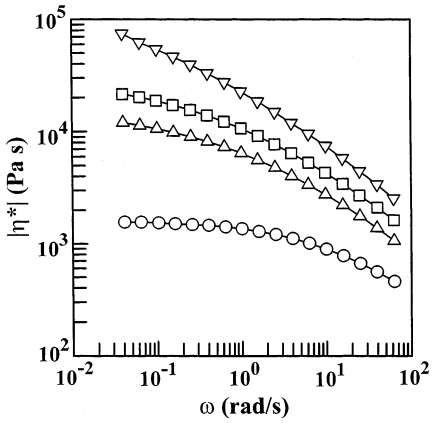

Figure 6. Plots of log $|\eta^*|$ vs log ω at 190 °C for (○) PP and $CaCO_3$-filled PP composites with varying concentrations of $CaCO_3$: (△) 10 wt % $CaCO_3$, (□) 20 wt % $CaCO_3$, and (▽) 40 wt % $CaCO_3$.

that highly filled thermoplastic molten polymers exhibit shear-thinning behavior (yield behavior) at very low shear rates in steady shear flow or at very low ω in oscillatory shear flow.[36] In Figure 6 we observe that the log $|\eta^*|$ vs log ω plot at low ω exhibits Newtonian behavior for neat PP and a very weak shear-thinning behavior for the 90/10 PP/$CaCO_3$ composite, but the intensity of shear-thinning behavior at low ω increases with an increase in $CaCO_3$ concentration to 20 and 40 wt %. In other words, the noticeable "yield behavior" of PP/$CaCO_3$ composites at low ω can be observed only when the concentration of $CaCO_3$ is sufficiently high. This observation explains, once again, why in Figure 2 and Figure 3b we observe that the 95/5 (SI-10/9)/Cloisite 30B nanocomposite at 115 °C and higher temperature (i.e., in the disordered state of SI-10/9) exhibits liquidlike behavior in the terminal region; i.e., the presence of 5 wt % Cloisite 30B (3.4 wt % net clay) in the 95/5 (SI-10/9)/Cloisite 30B nanocomposite is not sufficiently high to exhibit "yield behavior" at low ω.

Linear Dynamic Viscoelastic Properties of (SI-14/3-OH)/Cloisite 30B Nanocomposites. To facilitate our discussion below, we first present linear dynamic viscoelastic properties of neat diblock copolymer SI-14-3-OH. Figure 7a gives log G' vs log ω plots and Figure 7b gives log G'' vs log ω plots for SI-14/3-OH at various temperatures. In Figure 7a we observe that values of G' are very large at temperatures below 198 °C with a slope much less than 2 in the terminal region, indicating that the block copolymer exhibits linear dynamic viscoelasticity that represents a fluid somewhere between solidlike and liquidlike states, similar to that observed in Figure 1a for the lamella-forming block copolymer SI-10/9. As the temperature is increased to 198 °C, values of G' in the terminal region drop dramatically, and then the log G' vs log ω plot in the terminal region has a slope of 2, again very similar to that observed in Figure 1a for the lamella-forming block copolymer SI-10/9. The frequency dependence of G'' for SI-14/3-OH given in Figure 7b looks very complicated at temperatures below 198 °C, but log G'' vs log ω plots at 198 °C and higher temperatures show liquidlike behavior (a slope of 1).

Figure 8a gives log G' vs log ω plots and Figure 8b gives log G'' vs log ω plots for the 99/1 (SI-14/3-OH)/Cloisite 30B nanocomposite at various temperatures. It is seen in Figure 8 that, over the entire range of ω tested, both G' and G'' decrease as the temperature

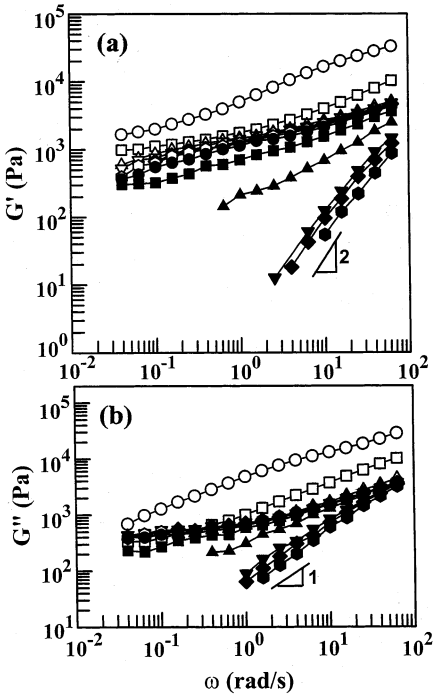

Figure 7. (a) Plots of log G' vs log ω and (b) log G'' vs log ω for SI-14/3-OH diblock copolymer at various temperatures: (○) 130, (□) 150, (△) 170, (▽) 180, (◇) 183, (⬡) 186, (●) 189, (■) 192, (▲) 195, (▼) 198, (◆) 200, and (⬢) 205 °C.

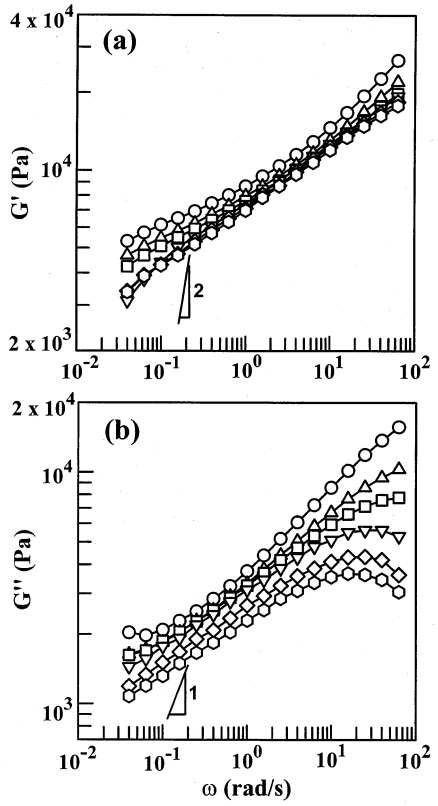

Figure 8. (a) Plots of log G' vs log ω and (b) log G'' vs log ω for 99/1 (SI-14/3-OH)/Cloisite 30B nanocomposite at various temperatures: (○) 170, (△) 185, (□) 200, (▽) 215, (◇) 230, and (⬡) 240 °C.

increases, but the temperature and frequency dependencies of both G' and G'' for the 99/1 (SI-14/3-OH)/Cloisite 30B nanocomposite are very different from those given in Figure 7 for the neat block copolymer

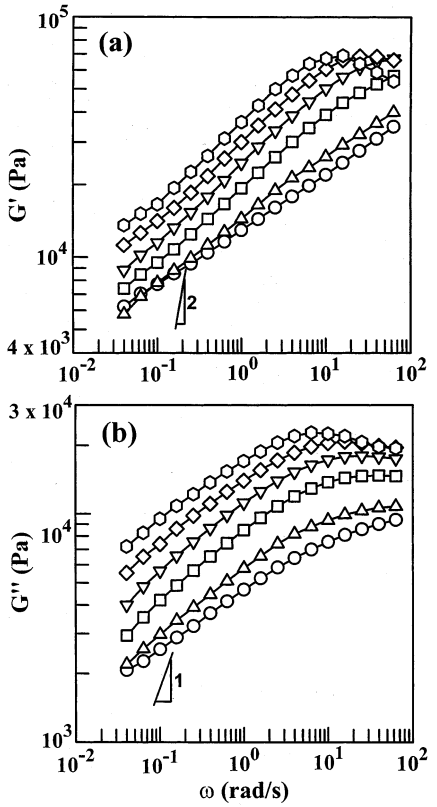

Figure 9. (a) Plots of log G' vs log ω and (b) log G'' vs log ω for 97/3 (SI-14/3-OH)/Cloisite 30B nanocomposite at various temperatures: (○) 170, (△) 185, (□) 200, (▽) 215, (◇) 230, and (⬡) 240 °C.

SI-14/3-OH and also given in Figure 2 for the 95/5 (SI-10/9)/Cloisite 30B nanocomposite. That is, referring to Figure 8, the addition of 1 wt % Cloisite 30B to SI-14/3-OH has changed so drastically the temperature dependence of G' and G'' of the 99/1 (SI-14/3-OH)/Cloisite 30B nanocomposite that we no longer can discern a temperature at which order−disorder transition (ODT) takes place.

Figure 9a gives log G' vs log ω plots and Figure 9b gives log G'' vs log ω plots for the 97/3 (SI-14/3-OH)/Cloisite 30B nanocomposite at various temperatures. A most interesting, unexpected feature of Figure 9 is that, over the entire range of ω tested, both G' and G'' increase as the temperature is increased when 3 wt % Cloisite 30B is added to SI-14/3-OH, a trend quite opposite to that observed in Figure 8 for the 99/1 (SI-14/3-OH)/Cloisite 30B nanocomposite and in Figure 2 for the 95/5 (SI-10/9)/Cloisite 30 nanocomposite. This observation indicates that 3 wt % Cloisite 30B in the 97/3 (SI-14/3-OH)/Cloisite 30B nanocomposite is sufficiently high enough to bring about strong interactions between the hydroxyl groups of SI-14/3-OH and the polar groups in MT2EtOH present on the surface of the silicate layers of the organoclay Cloisite 30B, whereas 1 wt % Cloisite 30B is not. Needless to state, such interactions cannot be expected when the block copolymer has no hydroxyl group, as is the case for the 95/5 (SI-10/9)/Cloisite 30B nanocomposite (see Figure 2).

Figure 10a gives log G' vs log ω plots and Figure 10b gives log G'' vs log ω plots for the 95/5 (SI-14/3-OH)/Cloisite 30B nanocomposite at various temperatures. Again, we observe that values of G' and G'' increase as the temperature is increased, very similar to that observed in Figure 9 for the 97/3 (SI-14/3-OH)/Cloisite

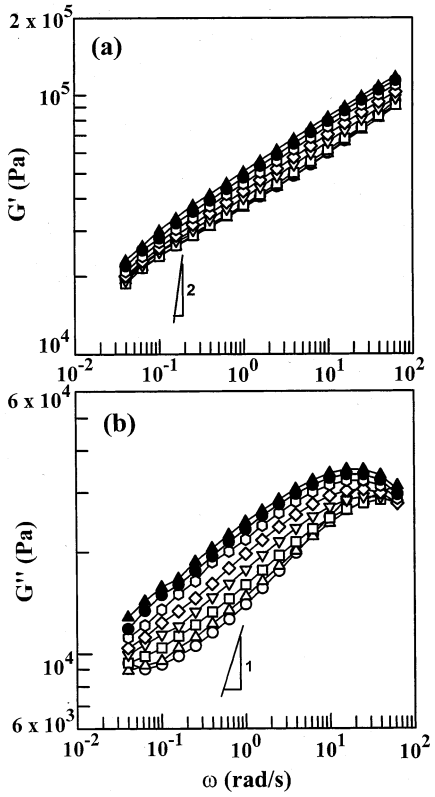

Figure 10. (a) Plots of log G' vs log ω and (b) log G'' vs log ω for 95/5 (SI-14/3-OH)/Cloisite 30B nanocomposite at various temperatures: (○) 170, (△) 180, (□) 190, (▽) 200, (◇) 210, (⬡) 220, (●) 230, and (▲) 240 °C.

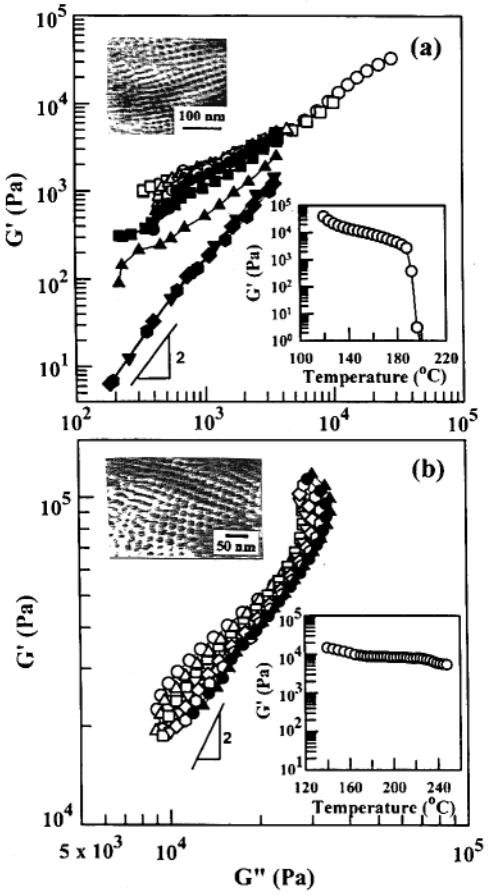

Figure 11. (a) Plots of log G' vs log G'' for SI-14/3-OH diblock copolymer at various temperatures: (○) 130, (□) 150, (△) 170, (▽) 180, (◇) 183, (⬡) 186, (●) 189, (■) 192, (▲) 195, (▼) 198, (◆) 200, and (⬢) 205 °C. The inset on the lower right side describes variations of G' with temperature during isochronal dynamic temperature sweep experiments at $\omega = 0.01$ rad/s, and the inset on the upper left side gives a TEM image of SI-14/3-OH taken at room temperature. (b) Plots of log G' vs log G'' for 95/5 (SI-14/3-OH)/Cloisite 30B nanocomposite at various temperatures: (○) 170, (△) 180, (□) 190, (▽) 200, (◇) 210, (⬡) 220, (●) 230, and (▲) 240 °C. The inset on the lower right side describes variations of G' with temperature during isochronal dynamic temperature sweep experiments at $\omega = 0.01$ rad/s, and the inset on the upper left side gives a TEM image of 95/5 (SI-14/3-OH)/Cloisite 30B nanocomposite taken after the specimen was quenched rapidly from 240 °C into ice/water.

30B nanocomposite. What remains to be answered is to elucidate the type of interaction(s) between the hydroxyl groups in SI-14/3-OH and the polar groups in MT2EtOH of Cloisite 30B in the 97/3 and 95/5 (SI-10/9)/Cloisite 30 nanocomposites.

Figure 11a gives log G' vs log G'' plots for neat diblock copolymer SI-14/3-OH at various temperatures, in which the inset on the lower right side describes the results of the isochronal dynamic temperature sweep experiments at $\omega = 0.01$ rad/s, and the inset on the upper left side gives a TEM image, taken at room temperature, of SI-14/3-OH that has hexagonally packed, cylindrical microdomains of PS. From the log G' vs log G'' plot given in Figure 11a we determine the T_{ODT} of SI-14/3-OH to be ca. 198 °C, which is very close to the temperature at which G', according to the inset, begins to drop precipitously.

Figure 11b gives log G' vs log G'' plots for the 95/5 (SI-14/3-OH)/Cloisite 30B nanocomposite at various temperatures, in which the inset on the lower right side describes the results of isochronal dynamic temperature sweep experiments at $\omega = 0.01$ rad/s, and the inset on the upper left side gives a TEM image, which was taken after the specimen was quenched rapidly from 240 °C into ice/water. It is seen that the block copolymer SI-14/3-OH in the nanocomposite still has hexagonally packed, cylindrical microdomains of PS. From the results of isochronal dynamic temperature sweep experiment we observe that values of G' stay more or less constant as the temperature is increased to ca. 250 °C, the highest experimental temperature employed; i.e., in the presence of 5 wt % Cloisite 30B the T_{ODT} of SI-14/3-OH has become so high that it could not be measured. In other words, in the presence of 5 wt % Cloisite 30B the hexagonally packed, cylindrical microdomains of PS in SI-14/3-OH persist even at such a high temperature, 250 °C. The same observation can be made from the log G' vs log G'' plots; namely, a close look at Figure 11b reveals that the log G' vs log G'' plot for the 95/5 (SI-14/3-OH)/Cloisite 30B nanocomposite continues to shift downward as the temperature is increased from 170 to 240 °C, the highest experimental temperature employed, during the dynamic frequency sweep experiment. Over the entire range of temperatures tested, the slope of the log G' vs log G'' plots is much less than 2, indicating that the block copolymer SI-14/3-OH is still in the ordered state. This means that the T_{ODT} of SI-14/3-OH in the 95/5 (SI-14/3-OH)/Cloisite 30B nanocomposite is much higher than 240 °C, in agreement with the conclusion drawn from the isochronal dynamic temperature sweep experiment, the inset of Figure 11b. Below we offer an explanation on the origin of the significant increase in T_{ODT} of SI-14/3-OH in the presence of Cloisite 30B.

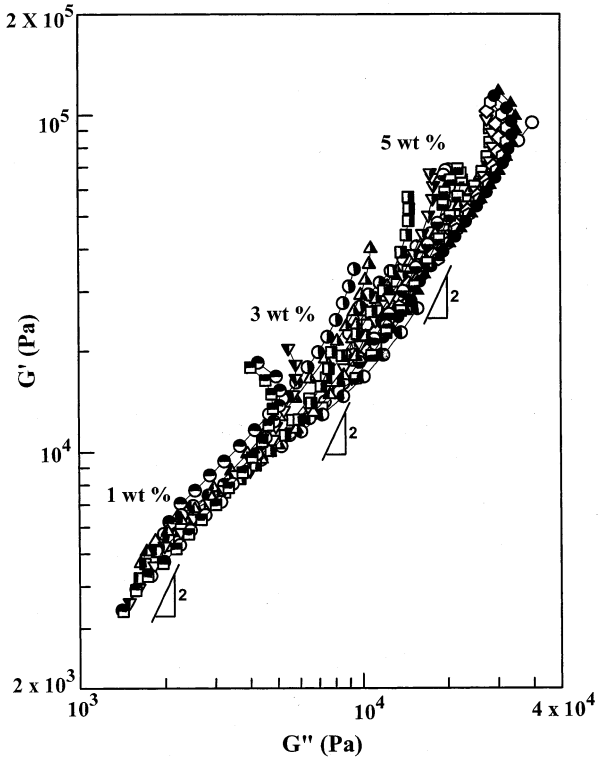

Figure 12. Plots of log G' vs log G'' for: (i) 99/1 (SI-14/3-OH)/Cloisite 30B nanocomposite at various temperatures: (◐) 170, (▲) 185, (◧) 200, (▼) 215, (◓) 230, and (⬒) 240 °C; (ii) 97/3 (SI-14/3-OH)/Cloisite 30B nanocomposite at various temperatures: (◑) 170, (▲) 185, (◨) 200, (▼) 215, (◒) 230, and (⬓) 240 °C; (iii) 95/5 (SI-14/3-OH)/Cloisite 30B nanocomposite at various temperatures: (○) 170, (△) 180, (□) 190, (▽) 200, (◇) 210, (⬠) 220, (●) 230, and (▲) 240 °C.

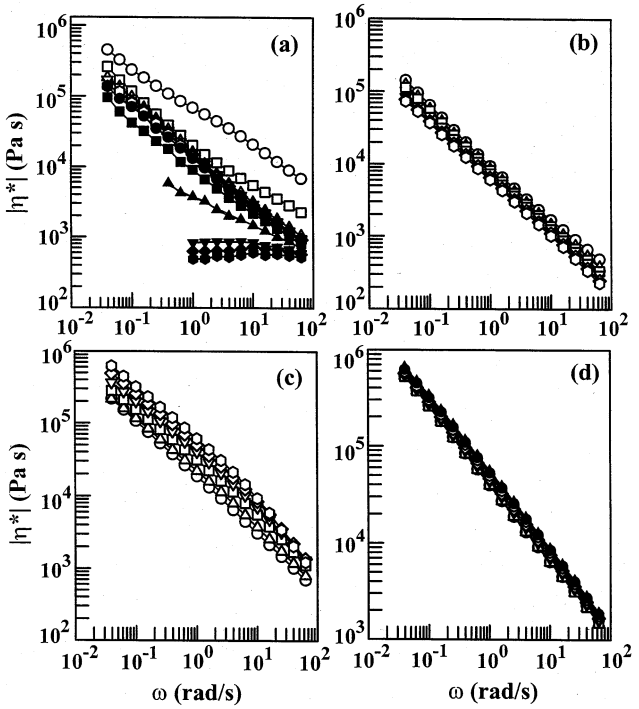

Figure 13. Plots of log $|\eta^*|$ vs log ω for: (a) SI-14/3-OH at (○) 130, (□) 150, (△) 170, (▽) 180, (◇) 183, (⬠) 186, (●) 189, (■) 192, (▲) 195, (▼) 198, (◆) 200, and (⬢) 205 °C; (b) 99/1 (SI-14/3-OH)/Cloisite 30B nanocomposite at (○) 170, (△) 185, (□) 200, (▽) 215, (◇) 230, and (⬠) 240 °C; (c) 97/3 (SI-14/3-OH)/Cloisite 30B nanocomposite at (○) 170, (△) 185, (□) 200, (▽) 215, (◇) 225, (⬠) and 240 °C; (d) 95/5 (SI-14/3-OH)/Cloisite 30B nanocomposite at (○) 170, (△) 180, (□) 190, (▽) 200, (◇) 210, (⬠) 220, (●) 230, and (▲) 240 °C.

The readers are reminded that the T_{ODT} of SI-10/9 in the *presence* of the organoclay Cloisite 30B has not changed (see Figure 3b). Thus, we speculate from Figure 11b for the 95/5 (SI-14/3-OH)/Cloisite 30B nanocomposite that there must have been strong interactions between the hydroxyl groups of SI-14/3-OH and the polar groups on the surface of the silicate layers of the organoclay Cloisite 30B, while no such interactions can occur when a block copolymer does not have functional groups, as is the case for the 95/5 (SI-10/9)/Cloisite 30B nanocomposite (see Figure 3b). The above observations seem to indicate that repulsive segment−segment interaction between PS and hydroxylated PI (PIOH) in the *presence* of the organoclay Cloisite 30B has increased considerably, compared to the repulsive segment−segment interaction between PS and PIOH in the *absence* of the organoclay.

Figure 12 gives log G' vs log G'' plots at temperatures ranging from 170 to 240 °C for the 99/1, 97/3, and 95/5 (SI-14/3-OH)/Cloisite 30B nanocomposites. It is clearly seen in Figure 12 that the log G' vs log G'' plots in the terminal region have a slope less than 2 for all three nanocomposites, indicating that the T_{ODT} of the block copolymer SI-14/3-OH in the respective nanocomposites is higher than 240 °C, the highest experimental temperature employed; i.e., all three nanocomposites retain hexagonally packed, cylindrical microdomains up to the highest experimental temperature employed (240 °C).

Figure 13 gives log $|\eta^*|$ vs log ω plots for (SI-14/3-OH)/Cloisite 30B nanocomposites with varying concentrations of Cloisite 30B at temperatures ranging from 170 to 240 °C. For comparison, also given in Figure 13 are log $|\eta^*|$ vs log ω plots for the neat block copolymer SI-14/3-OH. In Figure 13a we observe strong shear-thinning behavior at temperatures below 198 °C (T_{ODT}) due to the presence of hexagonally packed, cylindrical microdomains of PS in the SI-14/3-OH, but Newtonian behavior at 198 °C and higher temperatures (in the disordered state) over the entire range of ω tested for the neat block copolymer SI-14/3-OH. What is of great interest in Figure 13b−d is that all three nanocomposites exhibit very strong shear-thinning behavior over the entire range of ω and temperatures investigated. Notice in Figure 13b−d that the $|\eta^*|$ of the nanocomposite containing 1 wt % Cloisite 30B decreases with increasing temperature, while an opposite trend is observed as the concentration of Cloisite 30B is increased to 3 or 5 wt %. Again, the increasing trend of $|\eta^*|$ as the temperature is increased is attributable to the presence of interactions between the hydroxyl groups in SI-14/3-OH and the polar groups in MT2EtOH present on the surface of the silicate layers of the organoclay Cloisite 30B, leading to a significant degree of dispersion of clay aggregates. It is worth noting further in Figure 13 that the $|\eta^*|$ of the nanocomposites containing 3 or 5 wt % Cloisite 30B is much higher than that of the nanocomposite containing 1 wt % Cloisite 30B, and the difference in $|\eta^*|$ between the nanocomposite with 3 wt % Cloisite 30B and the nanocomposite with 5 wt % Cloisite 30B becomes smaller as the temperature is increased from 170 to 240 °C. The above observations seem to suggest that at 240 °C SI-14/3-OH may be not be as effective in exfoliating 5 wt % Cloisite 30B as 3 wt % Cloisite 30B.It should be emphasized that the strong shear-thinning behavior observed in Figure 13b−d for the (SI-14/3-OH)/

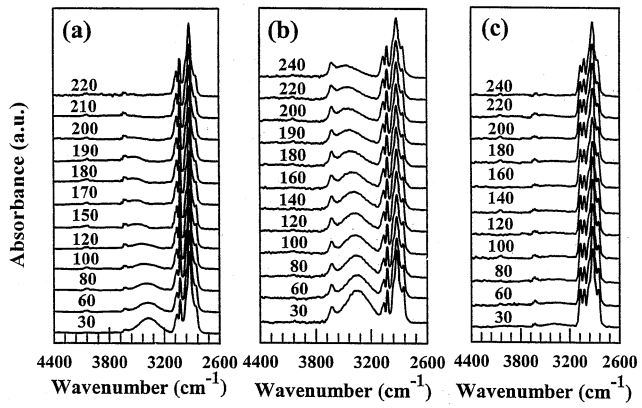

Figure 14. FTIR spectra at varying temperatures for (a) SI-14/3-OH, (b) 95/5 (SI-14/3-OH)/Cloisite 30B nanocomposite, and (c) 95/5 (SI-10/9)/Cloisite 30B nanocomposite.

Cloisite 30B nanocomposites has a physical origin, which is totally different from that associated with the shear-thinning behavior observed in Figure 6 for the 60/40 PP/$CaCO_3$ composite. The shear-thinning behavior observed in the 60/40 PP/$CaCO_3$ composite with such high (40 wt %) concentration of $CaCO_3$ (see Figure 6) is due to the presence of particle−particle interactions. If SI-14/3-OH had *no* hydroxyl group, the addition of such small amounts (1−5 wt %) of Cloisite 30B to the block copolymer could *not* possibly induce such a strong shear-thinning behavior in the (SI-14/3-OH)/Cloisite 30B nanocomposites.

Hydrogen Bonding in (SI-14/3-OH)/Cloisite 30B Nanocomposites. In an effort to search for evidence that may support or reject the postulations made above, in this study we have conducted in-situ FTIR experiment at various temperatures ranging from 30 to 240 °C for (i) neat block copolymer SI-14/3-OH, (ii) 95/5 (SI-14/3-OH)/Cloisite 30B nanocomposite, and (iii) 95/5 (SI-10/9)/Cloisite 30B nanocomposite, and the results are presented in Figure 14. Referring to Figure 14, hydrogen-bonded and free hydroxyl group appear at 3330 and 3630 cm^{-1}, respectively. The following observations are worth noting in Figure 14. (i) The area under the absorption band at about 3330 cm^{-1} for SI-14/3-OH is largest at 30 °C and then decreases as the temperature is increased. Notice in Figure 14a that the absorption band at about 3330 cm^{-1} virtually disappears completely at 200 °C, which is very close to the T_{ODT} of SI-14/3-OH (see Figure 7). The above observation indicates that the hydroxyl groups in the block copolymer form hydrogen bonding, and its strength is weakened with increasing temperature. (ii) In Figure 14b we observe that at 30 °C the area under the absorption band at about 3330 cm^{-1} for the 95/5 (SI-14/3-OH)/Cloisite 30B nanocomposite is indeed very large compared to that for the neat block copolymer SI-14/3-OH shown in Figure 14a. Most interestingly, the absorption band at about 3330 cm^{-1} for the 95/5 (SI-14/3-OH)/Cloisite 30B nanocomposite persists at temperatures as high as 240 °C, the highest experimental temperature employed. Notice that this is *not* the case for the neat block copolymer SI-14/3-OH (compare parts b and a of Figure 14). This observation suggests to us that there are strong hydrogen bonding between the hydroxyl groups in SI-14/3-OH and the hydroxyl groups in MT2EtOH of Cloisite 30B. (iii) In Figure 14c virtually no hydrogen bonding is discernible in the 95/5 (SI-10/9)/Cloisite 30B nanocomposite. This should not surprise us, because SI-10/9 does *not* have any hydroxyl groups. Thus, small amounts of hydroxyl groups present in the 5 wt % Cloisite 30B are diluted by the 95 wt % SI-10/9, making us virtually impossible to discern the presence of hydrogen bonding in the 95/5 (SI-10/9)/Cloisite 30B nanocomposite.

It is then very clear to us that the unusual linear dynamic viscoelastic properties observed in the 97/3 and 95/5 (SI-14/3-OH)/Cloisite 30B nanocomposites have originated from the presence of strong interactions, via hydrogen bonding, between the hydroxyl groups in SI-14/3-OH and the hydroxyl groups in MT2EtOH of Cloisite 30B.

Origin of the Observed Temperature Dependence of the Linear Dynamic Viscoelastic Properties of (SI-14/3-OH)/Cloisite 30B Nanocomposites. Now we offer a plausible mechanism(s) that might explain why G', G'', and $|\eta^*|$ increased when 3 or 5 wt % Cloisite 30B was added to the *functionalized* block copolymer, SI-14/3-OH, and why the T_{ODT} of SI-14/3-OH, in the *presence* of Cloisite 30B, increased considerably. Layered silicates have a large active surface area (700−800 m^2/g in the case of montmorillonite) and a moderate negative surface charge (cation exchange capacity). Upon replacing the hydrated metal cation from the interlayers in the pristine layered silicates with organic cations such as an alkyammonium, the layered silicate attains a hydrophobic/organophilic character and typically results in large interlayer spacing. As will be shown below, this is the reason that Cloisite 30B has larger interlayer spacing as determined from X-ray diffraction, compared to the *untreated* montmorillonite. Because the negative charge originates in the silicate layer, the cationic headgroups of the alkylammonium chloride molecule preferentially reside at the layer surface, and the aliphatic tail will radiate away from the surface. It should be remembered that Cloisite 30B has a hydroxyl group at the end of the aliphatic tail (bis-(2-hydroxyethyl)). Thus, when Cloisite 30B is mixed in solution, while vigorously stirring, with SI-14/3-OH, the hydroxyl group in SI-14/3-OH is expected to form *hydrogen bonds* with hydroxyl group of the aliphatic tail (in MT2EtOH) radiating from the layer surface, thereby enhancing compatibilization between SI-14/3-OH and organoclay platelets and thus enlarging the gallery distance between the organoclay platelets. The ability of the SI-14/3-OH molecules to enter between the organoclay platelets, owing to an enhanced compatibilization between SI-14/3-OH and Cloisite 30B due to hydrogen bonding, while vigorously stirring, will help disperse the organoclay aggregates and thus increase the surface areas available. In other words, the inherent incompatibility between the silicate layer and the isoprene chains, which exists when SI-10/9 *without* functional group is mixed with Cloisite 30B, is *modified* when SI-14/3-OH *with* functional group is mixed with Cloisite 30B, because the isoprene chains in SI-14/3-OH have hydroxyl groups that can form hydrogen bonds with the hydroxyl group present on the surface of the silicate layer of the organoclay Cloisite 30B. This is precisely the reason, we believe, why in the present study dramatic differences in the linear dynamic viscoelastic properties are observed between the 95/5 (SI-14/3-OH)/Cloisite 30B nanocomposite and the 95/5 (SI-10/9)/Cloisite 30B nanocomposite (compare Figure 10 with Figure 2, and Figure 11b with Figure 3b).

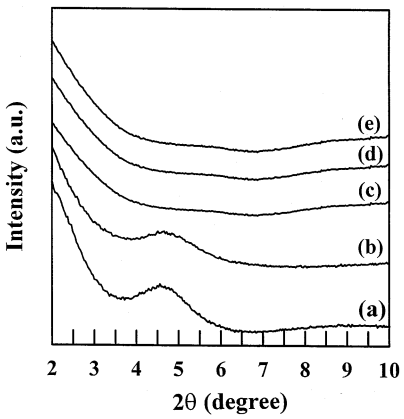

Figure 15. X-ray diffraction patterns for (a) Cloisite 30B, (b) 95/5 (SI-10/9)/Cloisite 30B nanocomposite, (c) 95/5 (SI-14/3-OH)/Cloisite 30B nanocomposite, (d) 97/3 (SI-14/3-OH)/Cloisite 30B nanocomposite, and (e) 99/1 (SI-14/3-OH)/Cloisite 30B nanocomposite.

One must still explain why G', G'', and $|\eta^*|$ in the 97/3 and 95/5 (SI-13/4-OH)/Cloisite 30B nanocomposites increase as the temperature is increased. We attribute this to an increase in the surface areas of dispersed silicate layers of the organoclay platelets as the temperature is increased. This is in part due to the decrease in the melt viscosity of SI-14/3-OH as the temperature is increased, thereby facilitating the dispersion (or breakup) of organoclay aggregates under oscillatory shearing motion. Consequently, as the number of sites available for hydrogen bonding between the polar group in MT2EtOH of Cloisite 30B and the hydroxyl group in SI-14/3-OH increases, the values of G', G'', and $|\eta^*|$ in the nanocomposites are expected to increase.

We now offer an explanation on the experimentally observed increase in the T_{ODT} of SI-14/3-OH in the presence of Cloisite 30B. In our previous paper,[29] we have shown from cloud point measurements that PS/PIOH mixtures are less miscible than PS/PI mixtures, and both PS/PIOH and PS/PI mixtures exhibit upper critical solution temperature (UCST). Further, using in-situ FTIR spectroscopy, we have also shown that the hydroxyl groups in SIOH form hydrogen bonds and that UCST increases as the extent of hydrogen bonding increases. Since both PS/PIOH and PS/PI mixtures exhibit UCST, the segment−segment interactions between PS and PIOH would be *more repulsive* than that between PS and PI. This means that the interaction parameter for PS/PIOH pair would be larger than that for PS/PI pair. It is then reasonable to expect that the segment−segment interactions between PS and PIOH would become more repulsive when the hydroxyl groups in SI-14/3-OH form hydrogen bonds with the hydroxyl groups in MT2EtOH of Cloisite 30B. It is well-established today that the T_{ODT} of a block copolymer depends on three factors:[37,38] (i) degree of polymerization, (ii) segment−segment interaction, and (iii) block composition (or block length ratio). Mean field theory[37,38] suggests that the T_{ODT} of block copolymer increases as the interaction parameter increases (i.e., the block components become more repulsive). Thus, we can conclude that the T_{ODT} of SI-14/3-OH in the presence of Cloisite 30B, where hydrogen bonding occurs between the hydroxyl groups in SI-14/3-OH and the polar group in MT2EtOH of Cloisite 30B, is expected to be higher than that of neat block copolymer SI-14/3-OH.

X-ray Diffraction of Organoclay and Its Nanocomposites with Block Copolymer. Figure 15 gives X-ray diffraction patterns of an organoclay Cloisite 30B and its nanocomposites with SI-10/9 and SI-14/3-OH. The X-ray diffraction in Figure 15 shows that Cloisite 30B has the intensity peak at $2\theta = 4.6°$, giving rise to a d_{001} spacing of 18.5 Å. The X-ray diffraction patterns given in Figure 15 indicate that the d_{001} spacing of the 95/5 (SI-10/9)/Cloisite 30B nanocomposite is *little* different from that of Cloisite 30B itself, suggesting that the block copolymer SI-10/9 has not intercalated the organoclay aggregates. On the other hand, in Figure 15 we observe *no* sharp reflections in the X-ray diffraction pattern of (SI-14/3-OH)/Cloisite 30B nanocomposites although a subtle difference seems to exist among the three different concentrations of Cloisite 30B. The lack of discernible intensity peak in Figure 15 for the three (SI-14/3-OH)/Cloisite 30B nanocomposites with varying amounts of Cloisite 30B seems to indicate that a significant degree of dispersion of the organoclay aggregates has occurred by the functionalized block copolymer SI-14/3-OH. As for the mechanism of dispersion of organoclay aggregates by SI-14/3-OH, the driving force is believed to have originated from the strong attractive interactions between the hydroxyl groups in SI-14/3-OH and the oxygen groups of the silicate layers of organoclay.[39]

Morphology of Block Copolymer/Organoclay Nanocomposites. Figure 16 gives TEM images of (a) 95/5 (SI-14/3-OH)/Cloisite 30B nanocomposite and (b) 95/5 (SI-10/9)/Cloisite 30B nanocomposite, where the dark areas represent the organoclay and the gray/white areas represent the block copolymer matrix. It is clearly seen from Figure 16 that SI-14/3-OH in the 95/5 (SI-14/3-OH)/Cloisite 30B nanocomposite has dispersed the organoclay aggregates fairly well, whereas SI-10/9 in the 95/5 (SI-10/9)/Cloisite 30B nanocomposite has not (i.e., large aggregates of organoclay are bundled together), indicating that the hydroxyl groups in SI-14/3-OH must have played the major role in dispersing (or breaking) the organoclay aggregates, leading to a significant degree of dispersion of the silicate layers of organoclay (Cloisite 30B) aggregates. It should be mentioned that the better dispersed the organoclay aggregates, the larger will be the surface areas of the silicate layers of organoclay that become available for interactions with the hydroxyl groups in SI-14/3-OH, which will in turn help increase the extent of dispersion of organoclay aggregates.

4. Concluding Remarks

In this study we have found that the functionalized diblock copolymer, SI-14/3-OH, is very effective to disperse the silicate layers of organoclay (Cloisite 30B) aggregates during solution blending, whereas unmodified SI diblock copolymer is not. Specifically, we have observed that both the dynamic storage and loss moduli of 97/3 and 95/5 (SI-14/3-OH)/Cloisite 30B nanocomposite are increased as the temperature is increased, while an opposite trend holds for the 95/5 (SI-10/9)/Cloisite 30B nanocomposite. The increasing trend of dynamic moduli of 97/3 and 95/5 (SI-14/3-OH)/Cloisite 30B nanocomposites with increasing temperature is believed due to an increase in the surface areas that are available for compatibilization, via hydrogen bonding, between the hydroxyl group in SI-14/3-OH and the polar groups in MT2EtOH residing at the surface of the silicate

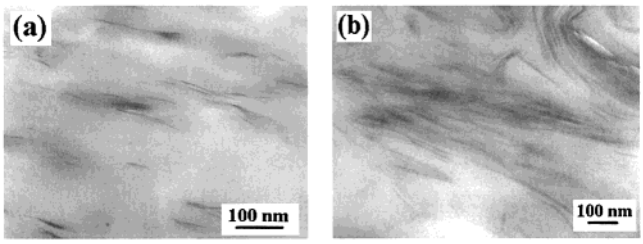

Figure 16. TEM images of (a) 95/5 (SI-14/3-OH)/Cloisite 30B nanocomposite and (b) 95/5(SI-10/9)/Cloisite 30B nanocomposite, where the dark areas represent the organoclay and the gray/white areas represent the block copolymer matrix.

layers of Cloisite 30B. Using FTIR spectroscopy, we have shown that hydrogen bonds between the hydroxyl group in SI-14/3-OH and the hydroxyl group in MT2EtOH of Cloisite 30B exist in the 95/5 (SI-14/3-OH)/Cloisite 30B nanocomposite at temperatures as high as 240 °C, the highest experimental temperature employed, whereas no hydrogen bonds exist in the 95/5 (SI-10/9)/Cloisite 30B nanocomposite. Since SI-10/9 does not have any polar functional groups, no interactions are expected between the SI-10/9 and Cloisite 30B, explaining the decreasing trend of dynamic moduli with increasing temperature. Further, we have observed that the T_{ODT} of SI-10/9 is *not* changed by the addition of Cloisite 30B, while the T_{ODT} of SI-14/3-OH is increased dramatically when Cloisite 30B is added. The observed increase in T_{ODT} of SI-14/3-OH in the 95/5 (SI-14/3-OH)/Cloisite 30B nanocomposite is attributable to the increase in *repulsive* segment−segment interaction between PS block and PIOH block that forms hydrogen bonds with the hydroxyl group in MT2EtOH of Cloisite 30B. In our recent paper,[29] we have demonstrated that hydroxylation of an SI diblock copolymer has increased its T_{ODT} dramatically, owing to a significant increase in repulsive segment−segment interaction between PS and PIOH, as compared to the segment−segment interaction between PS and PI.

The unusual linear dynamic viscoelastic properties of (SI-14/3-OH)/Cloisite 30B nanocomposites observed in this study are supported by two additional experimental observations: X-ray diffraction patterns and TEM images. Specifically, the d_{001} spacing of the (SI-10/9)/Cloisite 30B nanocomposite is found to be virtually the same as that of Cloisite 30B, whereas no sharp reflections in the X-ray diffraction patterns is found for the (SI-14/3-OH)/Cloisite 30B nanocomposites, suggesting that a good dispersion of organoclay aggregates took place during solution blending. TEM images show large organoclay aggregates in the (SI-10/9)/Cloisite 30B nanocomposite and a fairly well dispersed organoclay platelets in the (SI-14/3-OH)/Cloisite 30B nanocomposites. The objective of this study was to investigate the effectiveness of a functionalized block copolymer to disperse organoclay aggregates. We have achieved our objective using the hydroxylated SI diblock copolymer, SI-14/3-OH, prepared in this study.

However, from the point of view of mechanical properties, triblock copolymer is preferred to diblock copolymer, because the mechanical properties of a diblock copolymer are rather weak as compared to the mechanical properties of corresponding triblock copolymer having rigid end blocks. For instance, SIS triblock copolymer having rigid PS end blocks gives rise to strong mechanical properties as compared to SI diblock copolymer. In this regard, the mechanical properties of a functionalized SIS triblock copolymer, PS-*block*-PIOH-*block*-PS (SPIOHS triblock) copolymer, when mixed with an organoclay, are expected to be much stronger than the mechanical properties of an unmodified SIS triblock copolymer mixed with an organoclay. This subject is worth pursuing in future study.

To summarize, we have explained the experimentally observed increase in G', G'', and $|\eta^*|$ and also an increase in T_{ODT} for the (SI-14/3-OH)/Cloisite 30B nanocomposites in terms of the hydrogen bonding between the hydroxyl groups in SI-14/3-OH and the polar group in MT2EtOH of Cloisite 30B.

References and Notes

(1) Usuki, A.; Kawasumi, M.; Kojima, Y.; Fukushima, Y.; Okada, A.; Kurauchi, T.; Kamigaito, O. *J. Mater. Res.* **1993**, *8*, 1174.
(2) Yano, K.; Usuki, A.; Okada, A.; Kurauchi, T.; Kamigaito, O. *J. Polym. Sci., Polym. Chem. Ed.* **1993**, *31*, 2493.
(3) Kojima, Y.; Usuki, A.; Kawasumi, M.; Okada, A.; Kurauchi, T.; Kamigaito, O. *J. Polym. Sci., Polym. Chem. Ed.* **1993**, *31*, 983.
(4) Kojima, Y.; Usuki, A.; Kawasumi, M.; Okada, A.; Kurauchi, T.; Kamigaito, O.; Kaji, K. *J. Polym. Sci., Polym. Phys. Ed.* **1994**, *32*, 625.
(5) Kojima, Y.; Usuki, A.; Kawasumi, M.; Okada, A.; Kurauchi, T.; Kamigaito, O.; Kaji, K. *J. Polym. Sci., Polym. Phys. Ed.* **1995**, *33*, 1039.
(6) Reynaud, E.; Jouen, T.; Gauthier, C.; Vigier, G.; Varlet, J. *Polymer* **2001**, *42*, 8759.
(7) Kato, M.; Usuki, A.; Okada, A. *J. Appl. Polym. Sci.* **1997**, *66*, 1781.
(8) Kawasumi, M.; Hasegawa, N.; Kato, M.; Usuki, A.; Okada, A. *Macromolecules* **1997**, *30*, 6333.
(9) Hasegawa, N.; Kawasumi, M.; Kato, M.; Usuki, A.; Okada, A. *J. Appl. Polym. Sci.* **1998**, *67*, 87.
(10) Liu, X.; Wu, Q. *Polymer* **2001**, *42*, 10013.
(11) Nam, P. H.; Maiti, P.; Okamoto, M.; Kotaka, T.; Hasegawa, N.; Usuki, A. *Polymer* **2001**, *42*, 9633.
(12) Sikka, M.; Cerini, L. N.; Ghosh, S. S.; Winey, K. I. *J. Polym. Sci., Polym. Phys. Ed.* **1996**, *34*, 1443.
(13) Hasegawa, N.; Okamoto, H.; Kawasumi, M.; Usuki, A. *J. Appl. Polym. Sci.* **1999**, *74*, 3359.
(14) Ogata, N.; Kawakage, S.; Ohihara, T. *Polymer* **1997**, *38*, 5115.
(15) Liu, Y.-J.; Schindler, J. L.; DeGroot, D. C.; Kannewurf, C. R.; Hirpo, W.; Kanatzidis, M. G. *Chem. Mater.* **1996**, *8*, 525.
(16) Giannelis, E. P. *Appl. Organomet. Chem.* **1998**, *12*, 675.
(17) Giannelis, E. P.; Krishnamoorti, R.; Manias, E. *Adv. Polym. Sci.* **1999**, *138*, 107.
(18) Komori, Y.; Kuroda, K. In *Polymer-Organoclay Nanocomposites*; Pinnavaia, T. J., Beall, G. W., Eds.; Wiley: New York, 2000; p 3.
(19) Kato, M.; Usuki, A. In *Polymer-Organoclay Nanocomposites*; Pinnavaia, T. J., Beall, G. W., Eds.; Wiley: New York, 2000; p 97.
(20) Krishnamoorti, R.; Giannelis, E. P. *Macromolecules* **1997**, *30*, 4097.
(21) Lim, Y. T.; Park, O. O. *Rheol. Acta* **2001**, *40*, 220.
(22) Galgali, G.; Ramesh, C.; Lele, A. *Macromolecules* **2001**, *34*, 852.
(23) Solomon, M. J.; Almusallam, A. S.; Seefeldt, K. F.; Somwangthanaroj, A.; Varadan, P. *Macromolecules* **2001**, *34*, 1864.
(24) Ren, J.; Silva, A. S.; Krishnamoorti, R. *Macromolecules* **2000**, *33*, 3739.
(25) Krishnamoorti, R.; Ren, J.; Silva, A. S. *J. Chem. Phys.* **2001**, *114*, 4968.
(26) Physical Properties Bulletin from the Southern Clay Products, Inc.
(27) Brown, H. C. *Hydroboration*; Benjamin: New York, 1962.
(28) Chung, T. C.; Raate, M.; Berluche, E.; Schulz, D. N. *Macromolecules* **1988**, *21*, 1903.
(29) Lee, K. M.; Han, C. D. *Macromolecules* **2002**, *35*, 760.
(30) (a) Han, C. D.; Kim, J. *J. Polym. Sci., Polym. Phys. Ed.* **1987**, *25*, 1741. (b) Han, C. D.; Kim, J.; Kim, J. K. *Macromolecules* **1989**, *22*, 383. (c) Han, C. D.; Baek, D. M.; Kim, J. K. *Macromolecules* **1990**, *23*, 561.
(31) (a) Gouinlock, E. V.; Porter, R. S. *Polym. Eng. Sci.* **1977**, *17*, 535. (b) Chung, C. I.; Lin, M. I. *J. Polym. Sci., Polym. Phys. Ed.* **1978**, *16*, 545.

(32) Rosedale, J. H.; Bates, F. S. *Macromolecules* **1990**, *23*, 2329.
(33) Riise, B. L.; Fredrickson, G. H.; Larson, R. G.; Pearson, D. S. *Macromolecules* **1995**, *28*, 7653.
(34) Han, C. D.; Baek, D. M.; Kim, J. K.; Ogawa, T.; Sakamoto, N.; Hashimoto, T. *Macromolecules* **1995**, *28*, 5043.
(35) Han, C. D.; Vaidya, N. Y.; Kim, D.; Sakamoto, N.; Hashimoto, T. *Macromolecules* **2000**, *33*, 3767.
(36) Han, C. D. *Multiphase Flow in Polymer Processing*; Academic Press: New York, 1981; Chapter 3.
(37) Leibler, L. *Macromolecules* **1980**, *13*, 1602.
(38) Helfand, E.; Wasserman, Z. R. In *Developments in Block Copolymers*; Goodman, I., Ed.; Applied Science: New York, 1982; Chapter 4.
(39) Theng, B. K. G. *The Chemistry and Properties of Organoclay-Polymer Complexes*; Elsevier: New York, 1979.

MA020816F